Origin of the magnetoelectric effect in the $Cs_2FeCl_5{\cdot}D_2O$ compound

Oscar Fabelo,[1,*] J. Alberto Rodríguez-Velamazán,[1,2] Laura Canadillas-Delgado,[1,3] Lidia Mazzuca,[1] Javier Campo,[2] Ángel Millán,[2] Laurent C. Chapon,[1] and Juan Rodríguez-Carvajal[1]

[1]*Institut Laue Langevin, 71 Avenue des Martyrs, CS 20156, Cedex 9, Grenoble, 38042, France*

[2]*Instituto de Ciencia de Materiales de Aragón, CSIC-Universidad de Zaragoza, C/ Pedro Cerbuna 12, Zaragoza, 50009, Spain*

[3]*Centro Universitario de la Defensa de Zaragoza, Carretera de Huesca s/n. 50090 Zaragoza, Spain*

(Received 23 May 2017; revised manuscript received 21 July 2017; published 21 September 2017)

$Cs_2FeCl_5{\cdot}D_2O$ has been identified as a linear magnetoelectric material, although the correlation of this property with the magnetic structures of this compound has not been adequately studied. We have used single-crystal and powder neutron diffraction to obtain detailed information about its nuclear and magnetic structures. From the nuclear structure analysis, we describe the occurrence of a phase transition related to the reorganization of the $[FeCl_5{\cdot}D_2O]^{-2}$ ions and the Cs^+ counterion. The magnetic structure was determined at zero magnetic field at 1.8 K using single-crystal diffraction and its temperature evolution was recorded using powder diffraction. The symmetry analysis of the magnetic structure is compatible with the occurrence of the magnetoelectric effect. Moreover, the evolution of the magnetic structure as a function of the external magnetic field has also been studied. The reorientation of the magnetic moments under applied external field along the easy axis (*b* axis at low temperature) is compatible with the occurrence of a spin-flop transition. The application of a magnetic field below T_N compels the magnetic moments to flip from the *b* axis to the *ac* plane (with a small induced component along the *b* axis), for a critical magnetic field of ca. 1.2 T.

DOI: 10.1103/PhysRevB.96.104428

I. INTRODUCTION

Magnetoelectric (ME) materials, in which magnetization or polarization can be induced by, respectively, an electric or magnetic field, represent an attractive class of compounds with rich fundamental physics and potential applications in memory and logic devices [1]. Basically, two groups of ME materials can be distinguished: those where the ME effect is obtained due to the combination of different building blocks, each one responsible for the electrical and magnetic properties, respectively, and those where the ME effect is obtained in a single-phase compound. Within this second group there is a category of materials with linear ME coupling properties, such as $MnTiO_3$, $NdCrTiO_5$, $FeSb_2O_4$, or Cr_2O_3, in which electric polarization is induced by a special magnetic structure and increases linearly with increasing magnetic fields [2–5]. The ME effect couples both electric and magnetic fields, so that neither time reversal nor spatial inversion can be a symmetry operation of these systems; that is, linear ME effects can only occur in systems where both the spatial and the time inversion symmetry are broken.

In a previous paper we have reported the mechanism of multiferroicity of the $(ND_4)_2FeCl_5{\cdot}D_2O$ compound [6], which was explained by the so-called *inverse* Dzyaloshinskii-Moriya (DM) effect [7] or spin current mechanism, that predicts an electric polarization, $\mathbf{P}$, proportional to $\mathbf{r}_{ij} \times (\mathbf{S}_i \times \mathbf{S}_j)$, where $\mathbf{r}_{ij}$ is the vector connecting the nearest spins, $\mathbf{S}_i$ and $\mathbf{S}_j$. The exploration of other members of the $A_2FeX_5{\cdot}H_2O$ family, where *A* stands for an alkali metal or ammonium ion and *X* for a halide ion [8], has proven the occurrence of ME effects for some alkali-based compounds: $K_2FeCl_5{\cdot}H_2O$, $Rb_2FeCl_5{\cdot}H_2O$, and $Cs_2FeCl_5{\cdot}H_2O$. The K- and Rb-containing compounds crystallize in the *Pnma* orthorhombic space group [9,10], with a crystal structure at RT isomorphic to that of the ammonium-based multiferroic compound [6,11,12]. The magnetic structure of the $(ND_4)_2FeCl_5{\cdot}D_2O$ compound at zero field and 2 K shows an incommensurate cycloidal spin structure with a propagation vector $\mathbf{k} = (0,0,k_z)$, with $k_z = 0.2288(4)$ [6]. The magnetic moments are contained mostly in the *ac* plane with a small tilting angle of ca. 4° with respect to the *b* axis, and the cycloid propagates along the *c* axis. A recent work [13] shows the presence of weak second-order satellites, suggesting a non-negligible magnetostructural coupling. These results are rather different from those of the $K_2FeCl_5{\cdot}H_2O$ and $Rb_2FeCl_5{\cdot}H_2O$ compounds, which present commensurate, $\mathbf{k} = (0,0,0)$, antiferromagnetic structures and absence of ferroelectric signal at zero field. The magnetic structures at zero field of $K_2FeCl_5{\cdot}H_2O$ and $Rb_2FeCl_5{\cdot}H_2O$ compounds are described by the Shubnikov magnetic space group $Pn'm'a'$ belonging to the magnetic class $m'm'm'$ [14]. The magnetic moments of the Fe(III) ions are antiferromagnetically coupled within the zigzag chain running along the *b* axis, with the magnetic moments along the *a* direction; all the adjacent zigzag chains are in phase forming ferromagnetic *ac* planes, antiferromagnetically coupled along the *b* axis. These results are compatible with the occurrence of a magnetoelectric tensor where only the diagonal terms are nonzero and therefore the system can be described as linear ME [8].

The case of the $Cs_2FeCl_5{\cdot}H_2O$ compound is slightly different. The macroscopic measurements show that the system presents linear ME effect [8]; however, the origin of this behavior is not clear. In order to understand deeply the magnetoelectric correlations, the determination of the magnetic structure of this compound is mandatory.

In this paper, we investigate the temperature dependence of the nuclear structure using single-crystal neutron diffraction measurements. Below T_N we have determined the magnetic structure at zero magnetic field as well as the temperature

*fabelo@ill.fr

evolution of the magnetic structure by combining single-crystal and powder neutron diffraction. Finally, we present the magnetic structure determination above the magnetic-field-induced spin-flop transition, with the magnetic field applied along the *b* axis. All the magnetic structures have been analyzed using representational analysis, proving that the linear ME effect observed on the $Cs_2FeCl_5{\cdot}H_2O$ compound is compatible with the proposed magnetic structures.

II. EXPERIMENT

A. Materials

Deuterated reagents and solvents used in the synthesis were purchased from commercial sources and used without further purification.

B. Synthesis of the $Cs_2FeCl_5{\cdot}D_2O$ compound

Single crystals of $Cs_2FeCl_5{\cdot}D_2O$ of suitable size for neutron scattering were prepared by the slow evaporation technique under a controlled atmosphere. Stoichiometric quantities of CsCl and anhydrous $FeCl_3$ were dissolved in a minimum quantity of D_2O. The solution was filtered and left in a controlled atmosphere. Large red prismatic single crystals of $Cs_2FeCl_5{\cdot}D_2O$ were collected after several weeks (see Fig. S1 in the Supplemental Material [15]). The twinned or small-size crystals were collected and milled to obtain enough product to perform neutron powder diffraction experiments

C. Neutron diffraction instruments

Neutron diffraction measurements were performed with different instruments at Institut Laue Langevin (ILL, Grenoble, France): D1B and D2B, for powder diffraction measurements, and D9 and CYCLOPS for single-crystal diffraction studies.

Neutron powder diffraction experiments were carried out on the medium-resolution and high-flux D1B diffractometer and on the high-resolution D2B diffractometer, both equipped with variable temperature environment. The sample was contained in a Ø 5-mm cylindrical vanadium can and placed inside an Orange Cryostat or a closed-cycle cryostat device for D1B and D2B, respectively. High-resolution neutron diffraction patterns were acquired at room temperature (RT) and 45 K in D2B (wavelength 1.595 Å) in the 2θ range 0°–159.95° with a step size of 0.05°. The D1B instrument was operated with a wavelength of 2.521 Å, produced by its pyrolytic graphite monochromator. Graphite filters between the monochromator and the sample reduce the higher-order wavelength contamination, the proportion of $\lambda/2$ contamination being ca. 0.03%, which in the present case is in the limit of observation. Two high-flux neutron patterns were collected at 1.8 and 10 K, in the ordered and paramagnetic phases, respectively. The temperature evolution of the neutron diffraction pattern was followed from 1.8 to 10 K, with a heating rate of 0.04 K/min. Data reduction was carried out using LAMP software [16].

The single-crystal measurements (D9 and CYCLOPS) were carried out in a sample of $3 \times 4 \times 4\,mm^3$, approximately, which was mounted on a standard aluminum pin. The D9 instrument was equipped with a closed-cycle cryostat for low-temperature measurements. The instrument was operated in the four-circle configuration with a wavelength of 0.8409 Å for data collections at zero magnetic field at RT, 20 K (paramagnetic phase) and in the magnetically ordered phase (ca. 1.8 K). The measurements under external magnetic field were performed in D9 operating in "normal beam" geometry, working with the same wavelength and equipped with a vertical-field cryomagnet, which allows applying magnetic fields ranging from 0 to 6 T. The magnetic field was only applied along the *b* crystallographic direction (corresponding to the *a* axis of the high-temperature phase; see the crystal structure section). The crystal alignment was previously done using D9 working in a four-circle configuration.

The data collections in D9 consist of ω scans or ω-2θ scans. The program RACER [17] was used to integrate these scans and to correct them for the Lorentz factor. The crystal absorption corrections were made with the DATAP program [18], using an estimated absorption coefficient of $0.608\,cm^{-1}$, for a wavelength of 0.8409 Å, essentially due to the absorption cross section of the chlorine atoms [19].

The CYCLOPS measurements consisted of an exploration of the Laue patterns, at a specific orientation, as a function of the temperature. One hundred fifteen Laue diffraction patterns were collected during 15 min each with a difference of temperature of 1 K. Two different patterns after and before the nuclear structure transformation can be seen in Fig. S2 in the Supplemental Material [15].

The refinement of the nuclear and the magnetic structures was performed using the program FULLPROF. [20]. Due to the structural phase transition, the occurrence of two twin domains has been observed. These were included in the data reduction, and the ratio between both domains was refined giving rise to a proportion of 53%:47%. The models for the magnetic structure were deduced from the output of the program BASIREPS [21] included in the FULLPROF suite [20].

D. Neutron diffraction measurements

In order to determine an accurate structural model of the $Cs_2FeCl_5{\cdot}D_2O$ compound, in particular the deuterium positions, which are not easily determined from the x-ray experiments due to the low scattering power of these light atoms, neutron diffraction experiments were necessary [22]. Room temperature (RT) single-crystal neutron diffraction measurement was carried out at the D9 diffractometer. The obtained model was used as starting point to fit the low-temperature powder diffraction data collected on the D1B diffractometer. The fit of the data in the paramagnetic phase at low temperature with the room temperature model was not satisfactory, suggesting the occurrence of a nuclear phase transition, similar to that observed in the $(ND_4)_2FeCl_5{\cdot}D_2O$ compound [6]. This option was explored initially using the Laue diffractometer CYCLOPS [23] as a function of temperature and later on, with high-resolution powder neutron diffraction (see Figs. S2 and S3 in the Supplemental Material [15]). The comparison between different Laue images shows the appearance of new Bragg reflections below ca. 175 K, which is a fingerprint of the occurrence of a phase transition. The occurrence of this phase transition was corroborated through specific heat measurements, where a weak lambda peak was observed at 173 K (see Fig. S4 in the Supplemental

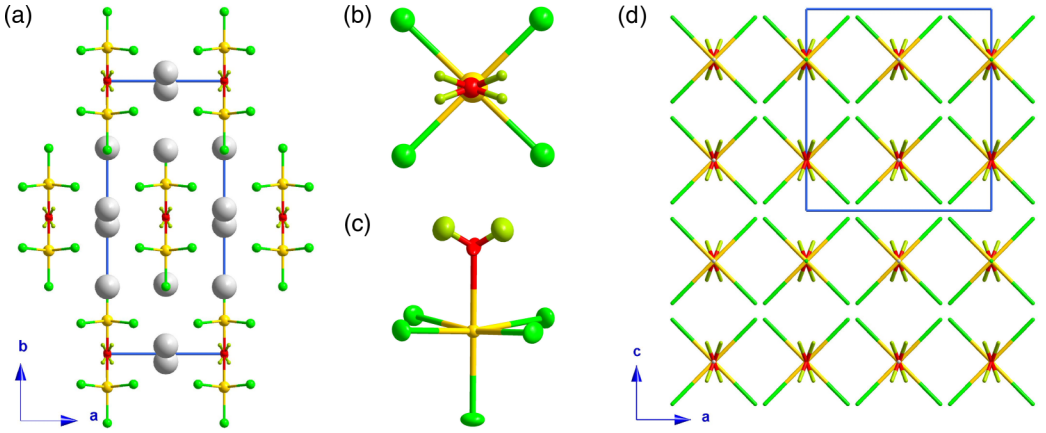

FIG. 1. (a) View along the c axis of the RT crystal structure. (b) Detail of the $[FeCl_5{\cdot}D_2O]$ unit where the two different positions of the coordination water molecule have been represented. (c) ORTEP representation of the $[FeCl_5{\cdot}D_2O]$ unit, where only one disordered position has been represented. (d) View of the crystal packing along the b axis. The Cs^+ ions have been omitted for the sake of clarity. The unit cell has been represented in blue. The iron, cesium, chlorine, oxygen, and deuterium ions have been represented in yellow, gray, green, red, and lime, respectively.

Material [15]). After the successful indexing of the low-temperature neutron powder diffraction, a full data set was collected at ca. 20 K on the D9 diffractometer in order to solve the crystal structure at low temperature in the paramagnetic phase. The magnetic structure determination at zero magnetic field and 1.8 K was carried out combining D1B and D9 data in a joint refinement.

III. RESULTS AND DISCUSSION

A. Crystal structure at high temperature (HT)

The title compound crystallizes in the orthorhombic $Cmcm$ space group with the following unit cell parameters: $a = 7.412302\,(3)$, $b = 17.3011\,(7)$, $c = 8.0742\,(3)$ Å, and $\alpha = \beta = \gamma = 90.0°$. The nuclear structure is built up from $[FeCl_5{\cdot}D_2O]^{2-}$ ionic units and Cs^+ counterions in a ratio of 1:2. The crystal structure can be seen as chains of $[FeCl_5{\cdot}D_2O]^{2-}$ units connected along the c axis through an extensive network of H bonds. Each chain is surrounded by six other chains following a stacking sequence ABAB along the b axis. The empty space between chains is filled by the Cs^+ counterions (see Fig. 1). The crystallographic details of the two phases (above and below the structural phase transition), including space groups and lattice parameters as well as some details of the data refinement, are shown in Table I. The atomic positions and thermal displacement parameter can be consulted in Table S1 or in the CIF files, data available in the Supplemental Material [15].

The Fe(III) atom is located in the intersection of two mirror planes, the first one perpendicular to the a axis and the second one perpendicular to the c axis. Moreover, a twofold axis is present along the b direction. The Fe(III) environment is filled by five chlorine ions and one coordination water molecule, which is disordered into two different positions, with an occupancy of 0.5. All the hydrogen atoms of this water molecule are involved in hydrogen bonds, giving rise to the mentioned chains along the c axis. The $[FeCl_5{\cdot}D_2O]^{2-}$ units form slightly distorted octahedra. The shortest Fe-Cl bond distances correspond to Cl(1), which is coordinated in *trans*- conformation with respect to the water molecule (see Table II).

The Fe-O(1w) bond distance is slightly elongated compared with the value previously reported for $(ND_4)_2FeCl_5{\cdot}D_2O$ compound and the *trans*-Fe-Cl(1) bond distance is slightly shorter. However, no significant difference has been observed for the bond distances in the equatorial plane. These deviations are related with the strength of the different hydrogen bonds at play. In this compound, the only hydrogen bonds are those related with the coordination water molecule [O(1w)-D$\cdots$Cl(2)], with a D$\cdots$Cl distance of 2.517(3) Å, notably longer compared with that previously reported for $(ND_4)_2FeCl_5{\cdot}D_2O$ [2.217(2) Å]. A detailed list with the geometrical parameters of all the possible H bonds can be consulted in Table III.

TABLE I. Crystal data and details of the structure determination for the complex 1.

Formula	$Cs_2FeCl_5{\cdot}D_2O$	
M	516.895	516.895
Crystal system	Orthorhombic	Monoclinic
Space group	$Cmcm$	$I2/c$
a (Å)	7.4123(3)	17.051(2)
b (Å)	17.3011(7)	7.3526(6)
c (Å)	8.0742(3)	16.136(1)
α (deg)	90.0	90.0
β (deg)	90.0	89.9505(4)
γ (deg)	90.0	90.0
V, (Å^3)	1035.44	2023.01733
Z	4	8
T (K)	300(2)	20(2)
$\rho_{calc}(g/cm^{-3})$	3.329	3.408
λ (Å)	0.8409	0.8409
Collected reflections	912	1802
Independent reflections	884	1507
$R_{int}(\%)$	5.69	7.01
$R_F(\%)$	6.64	5.21

TABLE II. Selected bond lengths (Å) and angles (deg) of compound 1. Symmetry codes: $a^1 : -x, y, z$; $b^1 : -x, -y, z-1/2$; $c^1 : -x-1/2, -y+1/2, z-1/2$; $a^2 : -x, \ y, -z-1/2$; $b^2 : -x-1/2, -y+1/2, -z-1/2$

300 K			
Fe(1)-Cl(1)	2.273(2)	Fe(1)-O(1)	2.175(4)
Fe(1)-Cl(2)	2.375(1)	O(1w)-D(1)	0.938(6)
		O(1w)-D($1a^1$)	0.943(6)
Fe(1)$\cdots$Fe($1b^1$)	5.841(2)	Fe(1)$\cdots$Fe($1c^1$)	7.0463(15)
20 K			
Fe(1)-Cl(1)	2.2862(17)	Fe(1)-Cl(5)	2.361(4)
Fe(1)-Cl(2)	2.398(4)	Fe(1)-O(1w)	2.181(2)
Fe(1)-Cl(3)	2.351(4)	O(1w)-D(1)	0.986(9)
Fe(1)-Cl(4)	2.400(4)	O(1w)-D(2)	0.964(8)
Fe(1)$\cdots$Fe($1a^2$)	5.790(5)	Fe(1)$\cdots$Fe($1b^2$)	6.954(4)

There are two crystallographically independent Cs^+ counterions, both located in 4*c* Wyckoff positions. However, from the crystal point of view, both behave very differently. The Cs(1), which is located at (0, 0.47044, 0.2500) and symmetry related positions, forms a zigzag chain with the adjacent Cs(1) along the *c* axis, while the Cs(2), located at (0, 0.75458, 0.2500) and symmetry related positions, lies in an almost perfect plane (see Fig. S5 in the Supplemental Material [15]).

The shortest Fe$\cdots$Fe distance connects iron atoms in the Fe(1)-O(1w)-D$\cdots$Cl(2)-Fe(1) zigzag chain running along the *c* axis, with a distance between metallic centers of 5.841(2) Å, notably shorter than those reported for $(ND_4)_2FeCl_5{\cdot}D_2O$ [6.457(1) Å]. The shortest interchain distance connects the Fe(III) atoms located at different *ac* planes, with a distance of 7.0463(15) Å, which is slightly longer than that observed for the $(ND_4)_2FeCl_5{\cdot}D_2O$ compound [6.8125(14) Å].

B. Crystal structure at low temperature (LT)

The neutron diffraction data below the phase transition temperature (ca. 175 K) reveal a nuclear phase transition from the *Cmcm* space group to $C2/c$. Although $C2/c$ is the standard space group, along this section, for the sake of the comparison, we are going to describe the crystal structure using the nonstandard $I2/c$ space group. Keeping invariant the origin of the unit cell at high temperature, the orthorhombic unit cell can be transformed into the monoclinic one by means of a simple axis permutation plus an axis doubling; then V^{LT} is almost equal to $2V^{RT}$ (*Cmcm* to $I2/c$ $\boldsymbol{a}' = \boldsymbol{b}, \boldsymbol{b}' = \boldsymbol{a}, \boldsymbol{c}' = -2\boldsymbol{c}$). The occurrence of this phase transition is confirmed by the appearance of new reflections that are not indexed in the orthorhombic space group.

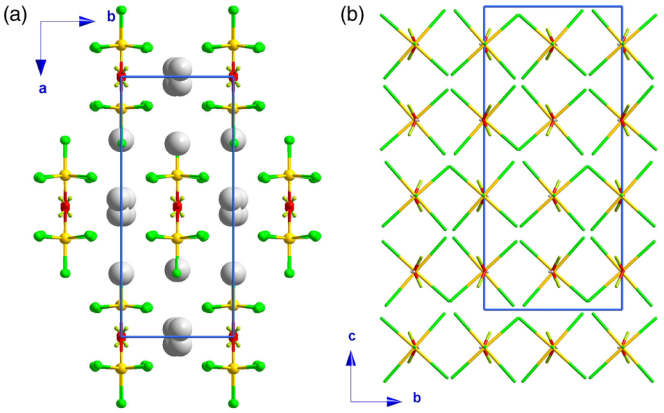

FIG. 2. (a) View along the *c* axis of the 20 K crystal structure. The unit cell has been represented in blue, while the iron, chlorine, oxygen, cesium, and deuterium ions have been represented in yellow, green, red, gray, and lime, respectively. (b) Detail of the ordered structure at low temperature along the *a* axis. The Cs^+ ions have been omitted for the sake of clarity.

The refined unit cell at 20 K is $a = 17.051(2)$, $b = 7.3526(6)$, $c = 16.136(1)$ Å; and $\alpha = 90.0°$, $\beta = 89.950(4)°$, and $\gamma = 90.0°$. The overall crystal structure remains very similar to the one above the phase transition: It can be seen as chains of $[FeCl_5{\cdot}D_2O]^{2-}$ units connected along the *c* axis through H bonds. The topology remains also equal, with each chain surrounded by six other chains (see Fig. 2). The symmetry breaking from orthorhombic to monoclinic produces instead notable changes in the Fe(III) site environment: The two mirror planes and the twofold axis that were located on Fe(III) in the orthorhombic phase are not present in the low-temperature phase. Therefore, the Fe(III) environment is now built up from five crystallographically independent chlorine ions and one coordination water molecule. A remarkable consequence of this symmetry breaking is the loss of the disorder in the coordination water molecule that was observed in the orthorhombic phase. This feature, together with the doubling of the *c* axis, causes the water molecules to follow a $+ - + -$ sequence along the *c* axis. The $+$ and $-$ signs have been used to represent the tilting angle of the water molecule, with $+$ if it is tilted up and–if it is tilted down with respect to the *ac* plane (see Fig. 2). As in the orthorhombic phase, all the hydrogen atoms are involved in hydrogen bonds.

TABLE III. Possible hydrogen bonds of compound 1.

300 K			
	Donor$\cdots$ acceptor (Å)	H$\cdots$ acceptor (Å)	Donor-H$\cdots$ acceptor (deg)
O(1w)-D$\cdots$Cl(2)	3.423(7)	2.517(3)	162.3(6)
20 K			
	Donor$\cdots$ acceptor (Å)	H$\cdots$ acceptor (Å)	Donor-H$\cdots$ acceptor (deg)
O(1w)-D(1)$\cdots$Cl(2)	3.279(6)	2.319(6)	164.5(5)
O(1w)-D(2)$\cdots$Cl(4)	3.281(6)	2.333(6)	167.5(5)

The $[FeCl_5 \cdot D_2O]^{2-}$ units present similar octahedral distortion; details of the Fe-Cl and Fe-Ow bond distances can be consulted in Table II. However, the hydrogen bonds [O(1w)-D $\cdots$ Cl(2/4)] present slightly shorter distances than that obtained for the orthorhombic phase, ca. 2.333(6) and 2.319(6) Å. A detailed list with the geometrical parameters of all the possible H bonds can be consulted in Table III. There are no important changes in the counterion network, only small shifts in the atomic positions due to the rearrangement of the coordination water molecule, which produces a small distortion of the Cs(1) zigzag chains (see Fig. S5 in the Supplemental Material [15]).

The shortest Fe $\cdots$ Fe distances connect iron atoms in the Fe(1)-O(1w)-D $\cdots$ Cl(4)-Fe(1) and Fe(1)-O(1w)-D $\cdots$ Cl(2)-Fe(1) zigzag chains running along the c axis, with distances between metallic centers of 5.790(5) and 5.795(5) Å, respectively, slightly shorter than in the orthorhombic phase [5.8399(14) Å]. The shortest interchain distance connects the Fe(III) atoms located in different bc planes, with a distance of 6.954(4) Å, slightly shorter than the distance obtained in the high-temperature phase [7.047(12) Å].

C. Magnetic structure at zero magnetic field

The neutron diffraction measurements at 1.8 K (below T_N) and zero magnetic field were carried out in D1B (powder) and D9 (single-crystal) instruments and analyzed in a joint refinement. The observed magnetic contribution, on top of nuclear reflections in the powder pattern, suggests that the magnetic reflections can be indexed with the propagation vector $\mathbf{k} = (0,0,0)$. This was confirmed by the survey of the reciprocal space in the single-crystal experiment, proving that the only compatible propagation vector is $\mathbf{k} = (0,0,0)$. A total of 1120 independent reflections were collected in D9 at 1.8 K (the same temperature of the data obtained in D1B). The temperature evolution of the sample was collected on D1B in the temperature range from 1.8 to 10 K (see Fig. 3). The onset of the appearance of magnetic reflections below ca. 6.6 K is in good agreement with T_N determined from the magnetometry measurements [8] and with the signal observed in the specific heat curve (Fig. S4 in the Supplemental Material [15]). In order to study the entropy related with the magnetic transition, we carried out a background correction by subtracting the phonon contribution (AT^3 term). The value of A was fixed to give no magnetic contribution well above the magnetic transition (above 20 K, $T > 3T_N$). The magnetic entropy was derived by integration of the Cp/T versus T plot up to 20 K, once the AT^3 contribution was subtracted. The value of the entropy associated to the magnetic transition approaches 14.7 J mol^{-1} K^{-1} (per Fe atom), remarkably close to 14.9 J mol^{-1} K^{-1}, the calculated value for $R\ln(2s+1)$ if $s = 5/2$, as is expected for a Fe(III) ion.

The representational analysis technique described by Bertaut was used to determine the possible magnetic structures compatible with the (nonstandard setting) $I2/c$ space group and propagation vector $\mathbf{k} = (0,0,0)$ [24]. Four irreducible representations (*irreps*) of the group G_k,(Γ_1,$-\Gamma_4$) and the corresponding set of basis vectors for each irreducible representation were determined using the program BASIREPS [21]. The magnetic representation Γ_M for the magnetic site [Wyckoff position $8f$ for Fe(1)] can be decomposed as a direct sum of *irreps* [see Eq. (1)]. In the present case, where $\mathbf{k} = (0,0,0)$, all the Fourier coefficients must be real and in

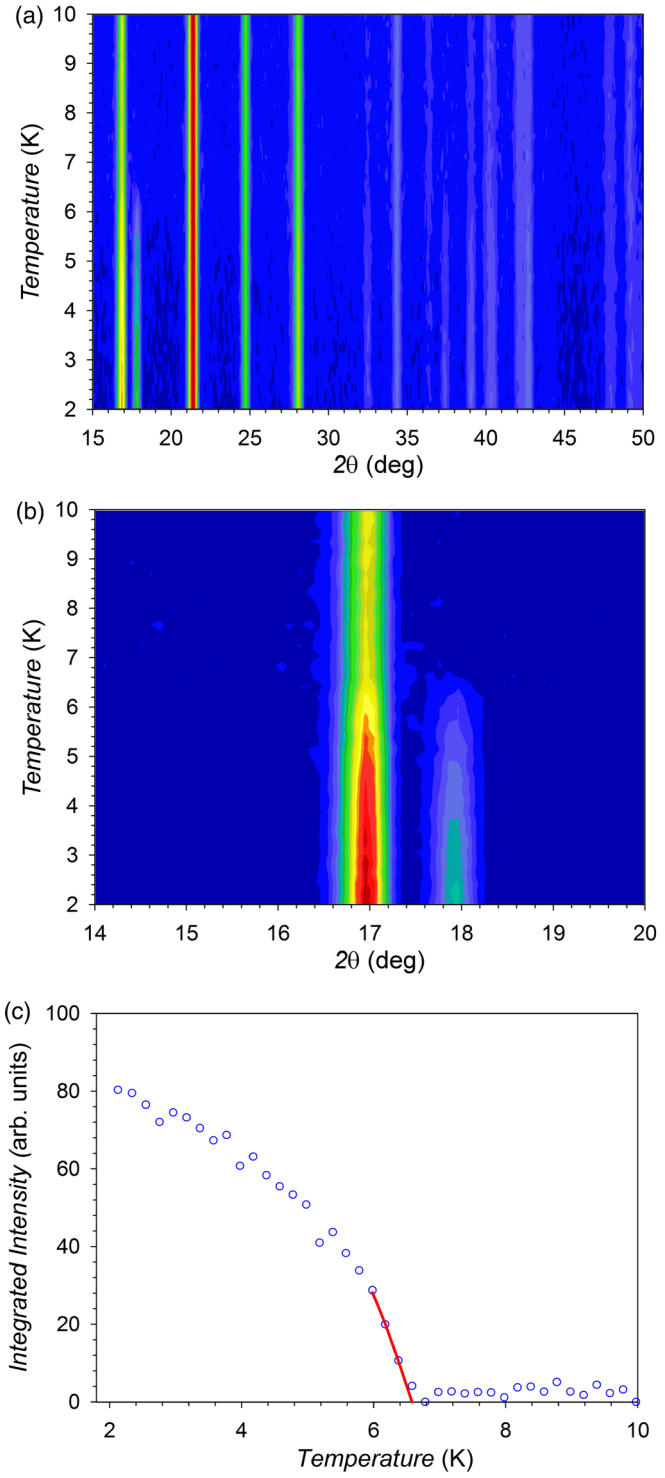

FIG. 3. (a) Mesh plot of the thermodiffractogram collected at D1B in the temperature range of 1.8–10 K. (b) Detail of the increase of intensity below T_N on the reflections (2 0 0) and (0 0 2) at 2θ values of 16.99° and 17.96° repectively. (c) Integrated intensity of the (0 0 2) magnetic reflection as a function of the temperature. The solid line represents the power-law fit of the data in the critical region (see main text).

TABLE IV. Irreducible representations for Fe(1) ion located at $(-0.12188, 0.0041, -0.3748)$ $8f$ Wyckoff position in the space group $I2/c$ with $\mathbf{k} = (0,0,0)$. The symmetry elements are written according to Seitz's notation. Magnetic moment components of the four *irreps* are also given. Atoms related by the centering translation $I(\frac{1}{2}, \frac{1}{2}, \frac{1}{2})$ are omitted.

	$(1\|000)$	$(2_{0y0}\|00p)$	$(-1\|000)$	$(m_{x0z}\|00p)$	Magnetic space group
Γ_1	1	1	1	1	$I2/c$
Γ_2	1	1	-1	-1	$I2/c'$
Γ_3	1	-1	1	-1	$I2'/c'$
Γ_4	1	-1	-1	1	$I2'/c$
			Magnetic moments		
$Fe_{8f}(1)$		Γ_1	Γ_2	Γ_3	Γ_4
	x, y, z	(u, v, w)	(u, v, w)	(u, v, w)	(u, v, w)
	$-x, y, -z+1/2$	$(-u, v, -w)$	$(-u, v, -w)$	$(u, -v, w)$	$(u, -v, w)$
	$-x, -y, -z$	(u, v, w)	$(-u, -v, -w)$	(u, v, w)	$(-u, -v, -w)$
	$x, -y, z+1/2$	$(-u, v, -w)$	$(u, -v, w)$	$(u, -v, w)$	$(-u, v, -w)$

principle all the *irreps* are possible solutions.

$$\Gamma_M(8f) = 3\Gamma_1 \oplus 3\Gamma_2 \oplus 3\Gamma_3 \oplus 3\Gamma_4. \quad (1)$$

A summary of the four possible *irreps* together with a detailed description of the basis vectors for the four possible *irreps* is shown in Table IV. The magnetic moments for the $8f$ Wyckoff position are obtained from the basis vectors as $\mathbf{m}_{8f}(1) = (u,v,w)$; therefore there are three degrees of freedom for the four possible magnetic structures. The Shubnikov group of each magnetic structure is written in the last column of Table IV.

The only irreducible representation that provides a satisfactory agreement between the calculated and the experimental diffraction data collected below T_N is Γ_4. From the joint powder/single-crystal refinement (see Fig. 4) we are able to obtain the relative orientation of the magnetic moments of the magnetic sites. The magnetic structure corresponds to a collinear antiferromagnetic (AF) arrangement, with the magnetic moments lying along the b axis. The refined magnetic moment is $\pm 4.39\,\mu_B$, value which is in agreement with previously reported Fe(III)-based compounds [14], and with the entropy value derived from heat capacity. Although the magnetic moments are not symmetry restricted to be along the b axis the refined components along the other directions are zero within the experimental error and were fixed in the last refinement (see Fig. 5). The refined magnetic structure gives rise to a magnetic model ($I2'/c$) which is a subgroup of the orthorhombic magnetic structure $Cmcm'$ predicted by Ackerman *et al.* [8]. However, this prediction did not take into account the occurrence of the structural phase transition at ca. 175 K that produces a breaking of symmetry from the orthorhombic $Cmcm$ to the monoclinic $I2/c$ space group, and

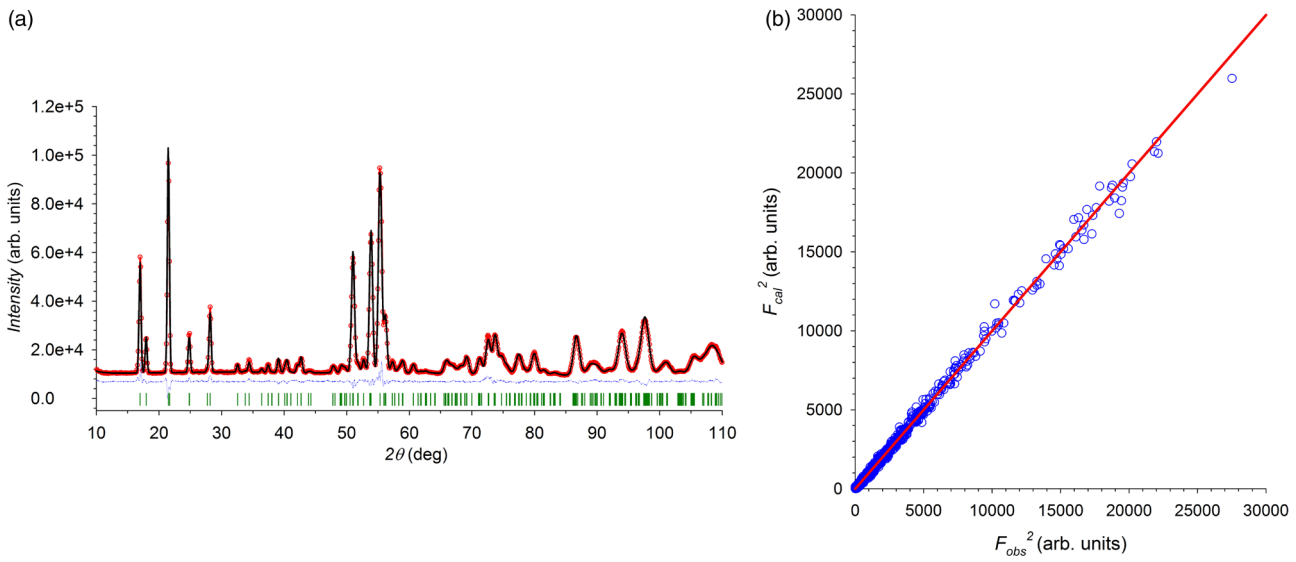

FIG. 4. (a) Experimental (open red circles) neutron powder diffraction data and calculated Rietveld refinement (black solid line) pattern for the $Cs_2FeCl_5{\cdot}D_2O$ compound (data collected at 1.8 K using the D1B instrument with $\lambda = 2.52$ Å). The difference between observed and calculated patterns has been represented as a blue line. The vertical green marks represent the position of the Bragg reflections. (b) Plot of the calculated versus observed square structure factors collected at 1.8 K in the D9 single-crystal diffractometer. The experimental data are represented as open blue circles and the ideal case ($F_{cal}{}^2 = F_{obs}{}^2$) is represented as a solid red line. The refinement has been done in the Shubnikov magnetic space group $I2'/c$, with the associated cell parameters $a = 17.0158(4)$, $b = 7.3394(2)$, and $c = 16.1049(4)$ Å; $\alpha = 90.0^\circ$, $\beta = 90.07(1)^\circ$, and $\gamma = 90.0^\circ$. The joint data refinement gives the following agreement factors: $R_B = 3.91\%$ for neutron powder diffraction and $R_F = 3.82\%$ for the single-crystal data.

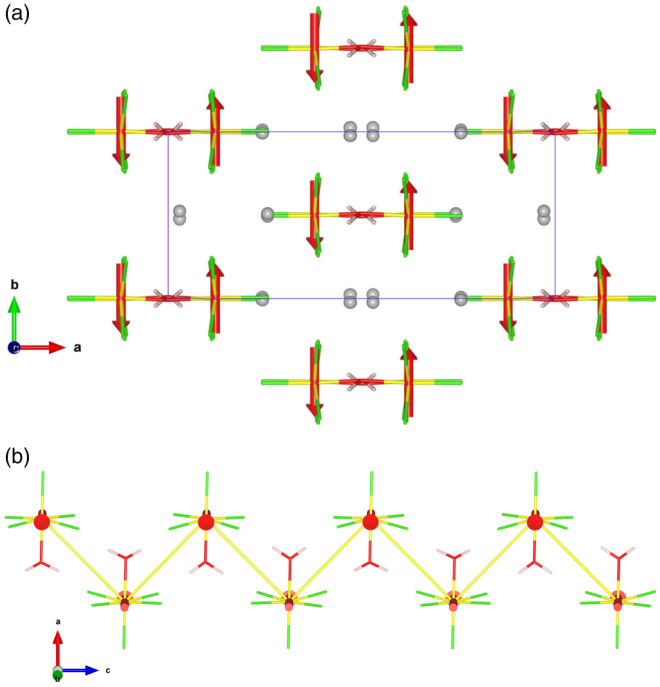

FIG. 5. (a) View of the magnetic structure at zero field of the $Cs_2FeCl_5{\cdot}D_2O$ compound along the c axis. (b) Detail of the antiferromagnetic zigzag chains running along the c axis. The yellow solid line is only a guide to the eye.

therefore the magnetic space group must be, more specifically, a subgroup of the paramagnetic group $I2/c1'$.

The evolution of the integrated intensity of the magnetic (0 0 2) reflection as a function of the temperature is shown in Fig. 3(b), while the evolution of the refined magnetic moment is shown in Fig. S6 in the Supplemental Material [15]. The integrated intensity of the (0 0 2) reflection was fitted in the critical region ($|T - T_N|/T_N < 0.1$) using a power law $I = I_0|T - T_N|^{2\beta}$ [solid line in Fig. 3(b)] giving rise to a critical exponent β of 0.38(2). This number should be taken with care, due to the low number of experimental points to fit in the critical region, but is in agreement with a 3D Heisenberg model, as expected for a Fe(III)-based compound. This result points to a non-negligible interaction between the adjacent zigzag chains running along the c axis (see Fig. 5).

The magnetic structure can be described as supramolecular Fe(III) chains connected through hydrogen bonds. The Fe $\cdots$ Fe chains connect iron atoms along the c axis following a zigzag sequence. The magnetic moment along these chains follows an antiferromagnetic arrangement. Each one of these chains is surrounded by six other chains, all of them magnetically equivalent (see Fig. 5). Alternatively, the magnetic structure can be described as a layered structure, the magnetic moments within the bc plane being ferromagnetically coupled, with the magnetic moments contained in the b axis. These layers are antiferromagnetically coupled along the a axis following an ABAB sequence (see Fig. 5).

D. Magnetic structure as a function of the magnetic field

The application of a weak magnetic field (below ca. 1.2 T) at temperatures below T_N along the b axis (a axis in the RT phase) produces an electric polarization along the a axis, while if the magnetic field is applied along the a axis, the electric polarization is observed along the b axis. The polarization along the a axis (magnetic field applied along the b axis), decreases noticeably when the external magnetic field approaches a critical field of ca. 1.2 T, while the components along the b and c axes arise. A detailed study of the electric polarization as a function of the applied external field in different crystal orientations can be consulted in Ref. [8].

The neutron diffraction measurements under magnetic field consisted firstly of an exploration of the reciprocal space at 1.8 K and 4.5 T. The only propagation vector compatible with the observations is $\mathbf{k} = (0,0,0)$. After the propagation vector determination, several reflections were followed as a function of the external magnetic field, $\mathbf{B}$ [from 0 to 5 T], at 1.8 K. The change in the intensity of the selected reflections is consistent with the occurrence of a spin-flop transition happening at ca. 1.2 T. The evolution of two reflections [(0 0 2) and (3 −1 0)] is shown in Fig. S7 in the Supplemental Material [15]. The variation of intensity from 0 to 1.2 T is not significant, although it deserves to be noted that even if the variation of intensity is not noticeable after applying an external magnetic field, the occurrence of electric polarization involves an underlying breaking of symmetry (structural and magnetic). After the spin-flop transition, above 1.2 T, the intensity of the magnetic reflections changes drastically, indicating a further breaking of the magnetic symmetry. Hereafter, we are going to evaluate the possible magnetic structures based on the symmetry analysis. This analysis can be extended to the nuclear structure, although, due to the low number of observations, we have described this last one in the parent $I2/c$ space group.

In the low-magnetic-field region (from 0 to 1.2 T), the changes in the magnetic intensities are subtle, which precludes an accurate determination in this region of a magnetic structure different from the one at zero field. However, the magnetic space group in this phase can be obtained from symmetry analysis. Taking into account the magnetic models at zero magnetic field, the four magnetic space groups corresponding to Γ_1−Γ_4 are $I2/c$(N.15.85), $I2/c'$(N.15.88), $I2'/c'$(N.15.89), and $I2'/c$(N.15.87), according to the Litvin numbering [25]. However, none of these magnetic space groups is compatible with the electric polarization observed in the macroscopic measurements. Therefore, a combination of irreducible representations is needed to explain the magnetoelectric effect observed in this phase. As the electric polarization occurs even at low magnetic fields, the magnetic structure in this phase should be a combination of the magnetic structure described at zero field with a second irreducible representation, allowing the occurrence of polarization. From the representational analysis described in the previous section, we can combine the Γ_4 irreducible representation (which describes the magnetic structure at zero magnetic field) with Γ_1, which is the only irreducible representation that allows a ferromagnetic component along the b axis, the direction of the external magnetic field. The magnetic structure in this region should be represented by the combination of Γ_1 and Γ_4, giving rise to the Ic space group (or Cc in standard notation), which is compatible with the macroscopic electric-polarization measurement.

In order to determine the magnetic structure above the spin-flop transition, 413 reflections were collected at 1.8 K and

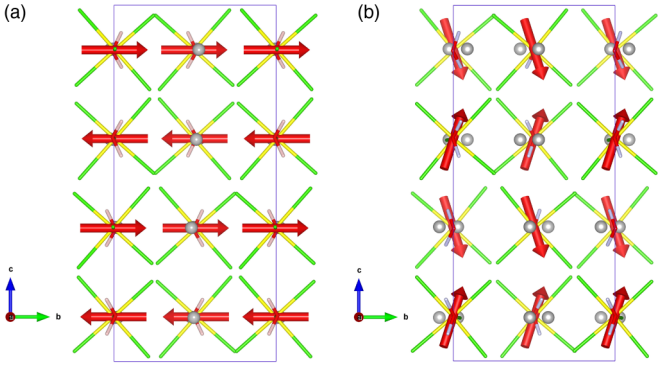

FIG. 6. Comparison views of the magnetic structure of $Cs_2FeCl_5{\cdot}D_2O$ at zero field (a) and at 4.5 T along the b axis (b) after the spin-flop transition.

4.5 T. The representational analysis described in the previous section is also valid for the current phase since the propagation vector remains $\mathbf{k} = (0,0,0)$. However, in this phase the system displays magnetoelectric behavior [8], and therefore neither time reversal nor spatial inversion can be symmetry operations of the system, which means that none of the zero-field *irrep*s is able to generate individually the experimentally observed macroscopic electric polarization, as was described for the low-magnetic-field phase.

In order to allow for the occurrence of electric polarization, a combination of magnetic models is again necessary. The list of subgroups of the paramagnetic $I2/c1'$ space group compatible with the macroscopic electric polarization is as follows: Ic' (N. 9.39), Ic (N. 9.37), $I2'$ (N. 5.15), $I2$ (N. 5.13), and $P1$ (N. 1.1). Moreover, the only irreducible representation allowing a ferromagnetic signal along the b axis is Γ_1: hence only the monoclinic space groups compatible with a field-induced component due to the application of an external field are the Ic and $I2$ space groups. Both magnetic space groups were used to refine the single-crystal data, although the best refinement was obtained using a combination of magnetic models belonging to the Γ_1 and Γ_2 irreducible representations (see Fig. S8 in the Supplemental Material [15]), described by the $I2$ (N. 5.13) magnetic space group. This means that a supplementary symmetry breaking occurs, due to the high field, with respect to the low-field phase that cannot be explained by a group-subgroup relation. The magnetic structure obtained can be described as a layered structure with the magnetic moments pillared along the c axis. The magnetic moments are shifted with respect to the zero-magnetic-field phase from the b axis to mainly the c axis (see Fig. 6). Different from the zero-field model, the magnetic structure under magnetic field has a non-negligible contribution along the other directions [a (ca. 1.07 μ_B) and b axis (ca. 2.2 μ_B)]. The components along the a and c axes are symmetry constrained to be antiferromagnetically coupled, but the contribution along the b axis is not compensated due to the application of the external magnetic field along this direction (see Fig. 6). Moreover, the comparison of the magnetic moment component along b in the two possible magnetic structures (Ic and $I2$) gives rise to 3.2(2) and 2.2(2) μ_B for the Ic and $I2$ magnetic space groups, respectively. For the Ic magnetic structure this value is far from the 1.9 μ_B expected from the magnetometry measurements, and therefore the Ic model can be discarded. Based on the refined magnetic model we can conclude that the crystal structure should also be described in the $I2$ space group but, since there are not enough observations to refine it, we have kept the parent $I2/c$ space group for the description of the crystal structure.

IV. CONCLUSIONS

In this work we have analyzed the nuclear and magnetic structures of the $Cs_2FeCl_5{\cdot}D_2O$ magnetoelectric compound by combining different neutron diffraction techniques. The occurrence of a structural phase transition has been determined using temperature-variable Laue diffraction and confirmed through specific heat measurements. The nuclear structure above and below the structural phase transition has been determined using monochromatic single-crystal neutron diffraction. The transformation of the space group from the orthorhombic $Cmcm$ to the monoclinic $C2/c$ (the nonstandard $I2/c$ space group has been used throughout the manuscript for the sake of easy comparison) was described. This transformation implies a doubling of the c axis associated with the ordering of the crystallization water molecules, which are disordered into two different orientations above the phase transition (ca. 175 K).

The accurate localization of the hydrogen (deuterium) atoms allows explaining the order-disorder phase transition as a consequence of the hydrogen bond network: The hydrogen bond distance thorough two $[FeCl_5{\cdot}D_2O]^{2-}$ units along the c axis is notably shorter in the monoclinic phase, giving rise to an ordered structure.

The determination of the magnetic structure at zero field has been done combining powder and single-crystal neutron diffraction data. The obtained magnetic space group is $I2'/c$, which has the spatial inversion as a symmetry operator but it is associated with time inversion in the action on spins. Therefore, the obtained magnetic model is compatible with the absence of electric polarization, as was observed in the macroscopic electric-polarization measurements; however, the presence of the $\bar{1}'$ operator ensures that it is linear magnetoelectric. The application of an external magnetic field, along the b axis, produces a field-induced ferromagnetic component. This produces a symmetry breaking, which is the responsible of the macroscopic electric polarization. However, the intensity of the magnetic reflections is not significantly modified with respect to the zero-field phase. This suggests that the magnetic model is not drastically changed with respect to the zero-field model. Symmetry analysis techniques have been used to propose a magnetic structure in the low-magnetic-field region (below 1.2 T). This analysis points to a phase transition from the nonpolar $I2'/c$ magnetic space group to the polar Ic.

The evolution of the magnetic reflections as a function of the external magnetic field proves that a spin-flop transition occurs at ca. 1.2 T at 1.8 K. This transition involves a reorientation of the magnetic moments from parallel to the b axis at zero field to mainly along the c axis at high field, with nonzero components along the a and b axes. The magnetic structure was refined in the $I2$ space group, which is compatible with both electric-polarization and magnetometry measurements.

The symmetry lowering below T_N confirms that the ferroelectricity observed in this compound is a direct consequence of the different magnetic structures as a function of the external magnetic field. The symmetry breakings resulting from these magnetic structures imply small shifts in the atoms' positions, which are the final responsible of the electric polarization. Therefore, from a crystallographic point of view, both the magnetic and crystal structures are concerned by the symmetry lowering, explaining the linear magnetoelectric behavior of the title compound above and below the spin-flop transition.

ACKNOWLEDGMENTS

The authors are grateful to the Institut Laue Langevin for the neutron beam-time allocated (doi:10.5291/ILL-DATA.5-41-829). Partial funding for this work is provided by the Ministerio de Economía y Competitividad (MINECO) through project MAT2015-68200-C2-2-P and Centro Universitario de la Defensa de Zaragoza through CUD 2013-17. Authors would like to acknowledge the use of Servicio General de Apoyo a la Investigación-SAI, Universidad de Zaragoza.

[1] M. Fiebig, Revival of the magnetoelectric effect, J. Phys. D: Appl. Phys. **38**, R123 (2005).

[2] N. Mufti, G. R. Blake, M. Mostovoy, S. Riyadi, A. A. Nugroho, and T. T. M. Palstra, Magnetoelectric coupling in $MnTiO_3$, Phys. Rev. B **83**, 104416 (2011).

[3] J. Hwang, E. S. Choi, H. D. Zhou, J. Lu, and P. Schlottmann, Magnetoelectric effect in $NdCrTiO_5$, Phys. Rev. B, **85**, 024415 (2012).

[4] A. Iyama, Y. Wakabayashi, N. Hanasaki, and T. Kimura, Magnetoelectric effect in $FeSb_2O_4$ single crystals, Jpn. J. Appl. Phys. **53**, 05FB02 (2014).

[5] A. Iyama and T. Kimura, Magnetoelectric hysteresis loops in Cr_2O_3 at room temperature, Phys. Rev. B **87**, 180408 (2013).

[6] J. A. Rodríguez-Velamazán, O. Fabelo, A. Millán, J. Campo, R. D. Johnson, and L. Chapon, Magnetically-induced ferroelectricity in the $(ND_4)_2[FeCl_5(D_2O)]$ molecular compound, Sci. Rep. **5**, 14475 (2015).

[7] I. Dzyaloshinskii, A thermodynamic theory of "weak" ferromagnetism of antiferromagnetics, J. Phys. Chem. Solids, **4**, 241 (1958); T. Moriya, Anisotropic Superexchange Interaction and Weak Ferromagnetism, Phys. Rev. **120**, 91 (1960); I. A. Sergienko and E. Dagotto, Role of the Dzyaloshinskii-Moriya interaction in multiferroic perovskites, Phys. Rev. B **73**, 094434 (2006).

[8] M. Ackermann, T. Lorenz, P. Becker, and L. Bohatý, Magnetoelectric properties of $A_2[FeCl_5(H_2O)]$ with A = K, Rb, Cs, J. Phys.: Condens. Matter **26**, 506002 (2014).

[9] C. J. O'Connor, B. S. Deaver, and E. Sinn, Crystal structures of $A_2FeCl_5.H_2O$ ($A = Rb^+$, Cs^+) and field dependent superconducting susceptometer measurements, J. Chem. Phys. **70**, 5161 (1979).

[10] J. N. McElearney and S. Merchant, Nonisomorphic antiferromagnetic behavior of two isomorphic salts: low-temperature heat capacities and magnetic susceptibilities of diammonium iron pentachloride monohydrate and dipotassium iron pentachloride monohydrate, Inorg. Chem. **17**, 1207 (1978).

[11] B. N. Figgis, C. L. Raston, R. P. Sharma, and A. H. White, Crystal structure of diammonium aquapentachloroferrate(III), Aust. J. Chem. **31**, 2717 (1978).

[12] M. Ackermann, D. Brüning, T. Lorenz, P. Becker, and L. Bohatý, Thermodynamic properties of the new multiferroic material $(NH_4)_2[FeCl_5(H_2O)]$, New J. Phys. **15**, 123001 (2013).

[13] W. Tian, H. Cao, J. Wang, F. Ye, M. Matsuda, J. Q. Yan, Y. Liu, V. O. Garlea, H. K. Agrawal, B. C. Chakoumakos, B. C. Sales, R. S. Fishman, and J. A. Fernandez-Baca, Spin-lattice coupling mediated multiferroicity in $(ND_4)_2FeCl_5.D_2O$, Phys. Rev. B **94**, 214405 (2016).

[14] M. Gabás, F. Palacio, J. Rodríguez-Carvajal, and D. Visser, Magnetic structures of the three-dimensional Heisenberg antiferromagnets $K_2FeCl_5.D_2O$ and $Rb_2FeCl_5.D_2O$, J. Phys.: Condens. Matter **7**, 4725 (1995); J. Campo, J. Luzón, F. Palacio, G. J. McIntyre, A. Millán, and A. R. Wildes, Understanding magnetic interactions in the series $A_2FeX_5.H_2O$ (A = K, Rb; X = Cl, Br). II. Inelastic neutron scattering and DFT, Phys. Rev. B **78**, 054415 (2008); J. Luzón, J. Campo, F. Palacio, G. J. McIntyre and A. Millán, Understanding magnetic interactions in the series $A_2FeX_5.H_2O$ (A=K, Rb; X=Cl, Br). I. Spin densities by polarized neutron diffraction and DFT calculations, *ibid.* **78**, 054414 (2008).

[15] See Supplemental Material at http://link.aps.org/supplemental/10.1103/PhysRevB.96.104428 for additional figures, tables, and CIF files.

[16] D. Richard, M. Ferrand, and G. J. Kearley, Analysis and Visualisation of Neutron-Scattering Data , J. Neutron Res. **4**, 33 (1996); LAMP, the Large Array Manipulation Program; see http://www.ill.fr/data_treat/lamp/lamp.html.

[17] M. S. Lehmann and F. K. Larsen, A method for location of the peaks in step-scan measured Bragg reflexions, Acta Crystallogr. A **30**, 580 (1974).

[18] P. Coppens, in *Crystallographic Computing*, edited by F. R. Ahmed (MunksgaardInternational Booksellers and Publishers Ltd., Copenhagen, 1979), pp. 255–270.

[19] H. Rauch and W. Waschkowski, *Neutron scattering lengths, in* ILL Neutron Data Booklet, 2nd ed., edited by A.-J. Dianoux and G. Lander (Institut Laue-Langevin, Grenoble, 2003); available on line at http://www.ill.eu.

[20] J. Rodríguez-Carvajal, Recent advances in magnetic structure determination by neutron powder diffraction, Physica B: Condensed Matter **192**, 55 (1993); The programs of the FULLPROF Suite and their corresponding documentation can be obtained from the Web at http://www.ill.eu/sites/fullprof/.

[21] J. Rodriguez-Carvajal, BASIREPS program, ILL, August, 2007. The program BASIREPS is included in the FullProf Suite and can be obtained from the Web at http://www.ill.eu/sites/fullprof/.

[22] P. J. Brown, A. G. Fox, E. N. Maslen, M. A. O'Keefe, and B. T. M. Willis, Intensity of diffracted intensitie, in *International Tables for Crystallography*, Vol. C, Chap. 6.1 (Wiley, 2006), pp. 554–595.

[23] B. Ouladdiaf, J. Archer, J. R. Allibon, P. Decarpentrie, M.-H. Lemée-Cailleau, J. Rodríguez-Carvajal, A. W. Hewat, S. York, D. Brau, and G. J. McIntyre, CYCLOPS - a reciprocal-space explorer based on CCD neutron detectors, J. Appl. Crystallogr. **44**, 392 (2011).

[24] E. F. Bertaut, *Magnetism*, edited by G. T. Rado and H. Shul (Academic Press, New York, 1963), Vol. III, Chap. 4.

[25] D. B. Litvin, Tables of crystallographic properties of magnetic space groups, Acta Crystallogr., Sect. A **64**, 419 (2008).